Effects of pilot injection parameters on low temperature combustion diesel engines equipped with solenoid injectors featuring conventional and rate-shaped main injection

EFFECTS OF PILOT INJECTION PARAMETERS ON LOW TEMPERATURE COMBUSTION DIESEL ENGINES EQUIPPED WITH SOLENOID INJECTORS FEATURING CONVENTIONAL AND RATE-SHAPED MAIN INJECTION

d'Ambrosio, S. , and Ferrari, A.*

Energy Department – Politecnico di Torino

C.so duca degli Abruzzi, 24, 10129, Torino, Italy.

ABSTRACT

The potential of pilot injection has been assessed on a low-temperature combustion diesel engine for automotive applications, which was characterized by a reduced compression-ratio, high *EGR* rates and postponed main injection timings. Dwell time sweeps have been carried out for pilot injections with distinct energizing times under different representative steady-state working conditions of the medium load and speed area of the New European Driving Cycle. The results of in-cylinder analyses of the pressure, heat-release rate, temperature and emissions are also presented.

Combustion noise has been shown to decrease significantly when the pilot injected mass increases, while it is scarcely affected by the dwell time between the pilot and main injections. The *HC*, *CO* and fuel consumption trends, with respect to both the pilot injection dwell time and mass, are in line with those of conventional combustion systems, and in particular decreasing trends occur as the pilot injection energizing time is increased. Furthermore, a reduced sensitivity of NO_x emissions to both dwell time and pilot injected mass has been found, compared to conventional combustion systems. Finally, it has been observed that soot emissions diminish as the energizing time is shortened, and their dependence on dwell time is influenced to a great extent by the presence of local zones with reduced air-to-fuel ratios within the cylinder. A combined analysis of the results of swirl sweeps and dwell time sweeps is here proposed as a methodology for the detection of any possible interference between pilot combustion burned gases and the main injected fuel.

The effect of pilot injection on engine performance and emissions has also been assessed in the presence of rate-shaped main injections. These main injection profiles have been implemented with solenoid injectors by designing the injection fusion between a pre injection shot, which is added after the pilot injection, and the main injection. This innovative strategy shows benefits, with respect to combustion noise, although it still results in a reduced impact on NO_x emissions. Furthermore, the brake specific fuel consumption and soot levels generally become worse than in the case of the simple

* Corresponding author e-mail address: alessandro.ferrari@polito.it.

pilot-main injection schedules. The injection fusion strategy has a significant impact on the soot versus dwell time dependence, which is influenced by the interference between the-main injection and pilot combustion.

Keywords: pilot injection; dwell time sweeps; swirl sweeps; injection fusion.

Highlights:

- The influence of the principal pilot injection parameters is discussed for low–temperature combustion systems.
- Swirl-sweep and dwell-time sweep results are combined to analyze soot emissions.
- The pilot injection effects are investigated in injection profiles featuring rate-shaped main injections.

1. INTRODUCTION

Both the pilot injected quantity (q_{pil}) and the dwell time (DT) between the pilot and main injections have been shown to exert a significant influence on the trade-off between engine-out emissions, combustion noise (CN) and fuel consumption in conventional diesel combustion systems at low to medium load and speed engine working conditions [1-4].

Since a reduction in the premixed combustion portion of the main injection makes the highest flame temperatures of the burned gases diminish, NO_x emissions generally reduce in pilot-main schedules, compared to single-injection strategies [5]. However, the pilot injection burns under premixed combustion conditions, and this constitutes an additional source of NO_x emissions. When large pilot injected quantities are applied, the increase in the NO_x amount, due to pilot combustion, can prevail over the decrease in the main combustion NO_x emissions, due to the shortened ignition delay and less intense premixed main combustion [6], and, as a consequence, NO_x emissions can augment overall for the strategy that implements the pilot shot. Furthermore, the earlier the pilot injection timing, which corresponds to a fixed pilot injected mass, the lower the heat release rate (HRR) peak of the pilot injection, and thus the more moderate the pilot combustion. This seems to suggest that an earlier pilot injection timing in conventional combustion systems limits the generation of the NO_x caused by pilot combustion [7], but aggravates the NO_x emissions produced in the main combustion.

Smoke emissions in pilot-main injections generally tend to increase at medium load and speed conditions, compared to single injections. In fact, the pilot injection leads to an increase in the in-cylinder temperature and a decrease in the oxygen concentration in the gases before the main injection has occurred, and both of these effects generally make the smoke emissions, produced during the main combustion, grow [7-9]. In general, the quantity of the pilot injection should be below a certain threshold (a general value of 4 mg can be prescribed) in order to contain the smoke amount

[10]. Soot emissions generally increase as the *DT* between the pilot and main injection is reduced [11]; this occurs for the same reasons that lead to the increase in the soot emissions that is detected when a pilot shot is added to the main injection. However, when the *DT* is very short, the main shot fuel is injected slightly before the burning of the pilot injection, and as a result, a lower rise in the temperature of the in-cylinder charge occurs and the ignition delay of the main injection tends to increase [12]. Furthermore, a small pilot injection, closely-coupled to the main injection ($DT \leq 500$ μs), can cause an increase in the velocity of the injector needle during the nozzle opening phase of the main injection, and this contributes to spray atomization enhancement [13]. Both these events can significantly improve the premixing phase of the main injected fuel with air and thus enable a reduction in the smoke emissions. On the other hand, the possible interference between the pilot combustion event and the main injection, which is more likely to occur for short *DT* values, can mask the benefits of both the increased ignition delay and the higher velocity of the needle at the beginning of the main injection, and this major interference can lead to an augment in the soot emissions.

The brake specific fuel consumption (*bsfc*) in the medium load and speed area of the New European Driving Cycle (*NEDC*) improves when a pilot injection is added to the main injection, and the improvement generally increases as the dwell time is reduced, because the pilot and main combustions are linked smoothly, and this has the potential of enhancing the combustion efficiency [14].

Finally, pilot injections are also effective in decreasing combustion noise: reductions of up to 5-8 dB are generally obtained in the *CN* value over the whole engine working area, even though the most obvious benefits are obtained at low loads and at idle [15-17]. Combustion noise normally decreases if the pilot injected mass augments, whereas the dependence of the *CN* on the pilot-main dwell time is more complex, because this trend is affected by the entity of the pilot injected mass, even though a decrease is generally observed as the dwell time is reduced [17].

The effects of pilot, post and multiple injection strategies on engine performance and emissions have been studied extensively at low to medium load and speed conditions in conventional diesel combustion modes with *EGR* fractions of up to 10-20% [18-21] and complete parametric analyses have been performed on several injection variables of the injection strategy [22]. In particular, the influence of the variations in the pilot injected quantity and the pilot-main dwell time has been investigated in detail for standard diesel combustion systems [23, 24].

The implementation of sophisticated injection strategies to control the PCCI combustion mode is a more recent challenge [25, 26]. Multiple injections are generally used in PCCI diesel engines to create a better air-fuel mixing charge with lowest possible wall-wetting [27], but there are few analyses in the literature about the effect of multiple injections on combustion noise and emissions in the presence of high EGR rates [25]. Multiple injections are usually focused on the extension of the high-load limits of the PCCI mode working area or on the emissions and noise of the PCCI engine [28]. The influence of an increase in the number of injection shots tends to be studied in general terms, and

87 comprehensive analyses on the effects of some key-injection parameters, such as dwell times and fuel quantities
88 injected in each shot, on engine performance are rare and very recent. Furthermore, investigations on multiple injections
89 often refer to PCCI engines fueled with gasoline [29] or alternative fuels, such as propane [30] or DME [31]. In
90 particular, great attention is being paid to the effects of pilot injection on engine performance in low-temperature
91 combustion systems characterized by heavy *EGR* rates and fueled with diesel oil [8, 14, 32-34].
92 In the current research investigation, dwell time sweeps have been studied within the 400 μs÷1600 μs range and at
93 different values of the pilot injected mass in pilot-main injection schedules, when high EGR rates are applied to a PCCI
94 engine fueled with diesel oil. Furthermore, an analysis of pilot injections with variable phasing and quantity in the PCCI
95 engine has also been performed for innovative injection schedules with a boot-like rate shaping of the main injection.
96 These sophisticated injection profiles have been implemented with direct-acting piezoelectric injectors, but there is a
97 lack of data in the literature about the effects of pilot injection timing and quantity on engine noise and emissions when
98 rate-shaped main injections, obtained by means of injection fusion techniques, are realized with solenoid injectors.
99 The experimental data, measured at a dynamometer cell, have been integrated with in-cylinder analyses, carried out
100 with a previously developed home-made combustion model [35], in order to improve the understanding of the main
101 physical phenomena.

102 2. EXPERIMENTAL FACILITIES AND ENGINE SET-UP.

103 The experimental tests have been carried out on the *AVL* dynamic test bed, installed at the Politecnico di Torino *ICE*
104 laboratories [32, 36]. The test facility is equipped with a raw exhaust-gas analyzer, which is basically made up of three
105 analyzer trains. One of these trains has been used, in the present investigation, to measure the NO_x, CO, CO_2, THC and
106 O_2 levels in the engine-out gases. A second train has been employed to detect the CO_2 concentrations in the inlet
107 manifold, in order to be able to calculate the *EGR* mass fraction, which is defined as $X_{EGR} = \dot{m}_{EGR}/(\dot{m}_{EGR} + \dot{m}_a)$ and has
108 been evaluated according to a previously developed procedure [37]. The third train is usually applied to detect the NO_x,
109 CO, CO_2, THC and O_2 levels downstream of the aftertreatment system, but these data have not been measured in the
110 present analysis since no aftertreatment device had been installed for the performed tests.
111 As far as the particulate matter (*PM*) measurement is concerned, the dynamic test bed is equipped with the following
112 instruments: *AVL 415S* smokemeter, *AVL 439* opacimeter and *AVL SPC472* Smart Sampler. Finally, an '*AVL KMA*
113 4000 Methanol' measuring system continuously meters the engine fuel consumption over the 0.28-110 kg/h range with
114 a reading accuracy of 0.1% for diesel fuel.
115 The tested engine, the main features of which are reported in Table 1, is a Euro 5 engine, fueled with conventional
116 diesel oil, by means of hydraulically-actuated solenoid injectors of the latest generation. The twin-stage turbocharger is

used to increase the full load *bmep* to 25 bar and engine transient performance, but it is not fully exploited in most of the *NEDC* area or in the entire PCCI working zone that occurs at low load and speed conditions.

A high-frequency piezoelectric transducer has been installed on the engine cylinder head to measure the pressure time-history of the gases in one of the cylinders, and another high-frequency piezoresistive transducer has been used to detect the pressure levels in the inlet runner of the same cylinder in order to reference the in-cylinder pressure. An *AVL 365C* crank-shaft driven encoder generates the time base for an automatic data-acquisition system, which is managed by *AVL Indicom* software, in order to allow both the online analysis of the indicated cycle and data storage operation for post-processing with a three-zone combustion diagnostic tool. In this tool [35], the combustion chamber content is divided into three zones: a fuel zone, an unburned gas zone (containing fresh-air, residual gas and *EGR*) and a burned gas zone, obtained from a global stoichiometric combustion process. Ordinary differential mass and energy conservation equations are applied to the three zones and are solved numerically, while the experimental in-cylinder pressure and injected flow-rate time histories are provided as input data. The model allows the temperatures of the three zones to be calculated as functions of the crank angle. Furthermore, thermal and prompt *NO* mechanisms are implemented in the simulation code, according to the Zeldovich and Fenimore submodels, respectively. Soot formation is modeled [38] by means of an expression that considers the mean air-fuel ratio over the combustion interval, whereas the soot oxidation rate is modeled using an empirical formula, based on the temperature of the burned gas zone.

3. EFFECT OF THE PILOT INJECTION PARAMETERS ON LOW TEMPERATURE COMBUSTION SYSTEMS

Figures 1-6 report the *bsfc*, *CN* and engine-out emission experimental data, plotted as functions of the dwell time between the pilot and main injection shots in the 400 μs<*DT*<1200 μs range, for the *n*=2000 rpm and *bmep*= 5 bar (2000x5) engine working condition. The lower limit of the dwell time was set at 400 μs, because the pilot injection can hydraulically interfere directly on the main injection dynamics and fusion phenomena can occur below this threshold [9]. Three different quantities have been considered for the pilot injection in each graph, and each quantity corresponds to a distinct value of the energizing time of the pilot injection (ET_{pil}). The *DT* sweeps have been performed by maintaining all the other engine parameters constant, with the exception of the main injection energizing time (ET_{main}), which is changed by the test bed control system in order to maintain the desired *bmep*.

Table 2 reports the main test conditions under which the *DT* sweeps have been carried out: the variations in *MFB50* are within 1°CA during each *DT* sweep, and are therefore not significant. The electrical start angle of the pilot injection (SOI_{pil}) is not reported because it was made to vary in the *DT* sweep tests. However, it can easily be calculated on the

basis of the DT and the ET_{pil} values (both expressed in μs), according to the $SOI_{pil}=SOI_{main}-6\cdot10^{-6}n\ (ET_{pil}+DT)$ formula, where n is the engine speed (in *rev/min*) and SOI_{main} (°CA ATDC) is the main injection start angle.

The adopted X_{EGR} is around 40%, that is, much higher than the values usually implemented in conventional diesel combustion systems (20-25%) at medium load and speed conditions. Furthermore, SOI_{main} is postponed in the implemented calibration and this condition, together with the application of a low compression ratio (ε=16.3 in Table 1) engine, is suitable for low-temperature combustion systems. As no aftertreatment device was installed to reduce engine-out NO_x emissions, the retarded main injection pulse is useful to decrease peak in-cylinder temperatures and inhibit NO_x formation.

The experimental in-cylinder pressure (p_{cyl}) crankshaft angle based distributions and the model based heat release rate traces, which refer to three combinations of DT and ET values (DT=400 μs and ET_{pil}=210 μs, DT=1200 μs and ET_{pil}=210 μs and DT=1200 μs and ET_{pil}=160 μs, respectively) are reported in Figs. 7 and 8, together with the schematic injected flow-rate.

The high brake specific fuel consumption shown in Fig. 1 can be attributed to the abovementioned postponed main injection: in fact, a delayed SOI_{main} improves NO_x, but leads to a deterioration of *bsfc*, due to the NO_x-*bsfc* trade-off. Brake specific fuel consumption generally becomes worse as the dwell time between the pilot and main injection is increased. In fact, a reduced DT makes the overall combustion occur over a shorter time, and this determines a decrease in *bsfc*. Furthermore, when either q_{pil} is increased (by enlarging ET_{pil}) or DT is reduced, the pilot and main combustions are linked more smoothly, or are at least closer (cf. Fig. 8), and this situation has been verified to induce a higher mean temperature of the in-cylinder gases over the main combustion event, thus enhancing combustion efficiency.

The dependence of the combustion noise on both DT and q_{pil} has been outlined in Fig. 2. The results plotted with respect to ET_{pil} are in line with those reported in the literature for moderate *EGR* rates [8]: the higher the ET_{pil}, i.e. q_{pil}, the lower the *CN*. On the other hand, the combustion noise reduces for increasing DT, and this result is consistent with the model data given in Fig. 8, where it can be observed that the *HRR* peak that refers to the premixed phase of the main combustion becomes more vigorous as DT reduces (cf. traces at ET_{pil}=210 μs to assess the effect of DT on *CN* and traces at DT=1200 μs to evaluate the influence of ET_{pil} on *CN*). It is possible to note that the schematic injection rate given in Fig. 8 starts at a higher θ angle than the 0.5 °CA ATDC reported in Table 2. In fact, the angular position in Table 2 refers to the start of the electrical command, whereas Fig. 8 shows the schematic injected flow-rate. The delay between the command and the actuation is related to the injector nozzle opening delay, which is generally a function of *ET* and the rail pressure level [39].

It can be observed, in Figs. 3 and 4, that the engine-out *HC* and *CO* emissions tend to increase as DT is augmented from 400 μs to 1200 μs; furthermore, the higher the value of ET_{pil} , the lower the *HC* and *CO* emissions are in general. These

177 data are in agreement with those reported in other works [14, 40], which refer to moderate *EGR* conditions in
178 conventional diesel combustion systems. If either the pilot injection quantity becomes lower or the pilot injection timing
179 occurs earlier, the occurrence of overmixing is more likely, and this causes an increase in the *HC* emissions. In other
180 words, when the *DT* is increased (the SOI_{main} is approximately 0.5°CA ATDC, cf. Table 2), the pilot fuel is injected into
181 an increasingly cooler environment, and this leads to an augment in the autoignition delay of the pilot injected fuel,
182 which in turn promotes an overmixing of the fuel with air. The augment in the autoignition delay of the pilot injected
183 fuel for increasing *DT* is confirmed from a combined analysis of the *HRR* traces and schematic injected flow-rates
184 shown in Fig. 8. Furthermore, if the pilot injected mass reduces, the *HC* and *CO* emissions increase, because of the
185 lower local equivalence ratio (ϕ) values pertaining to the pre-reactions of the pilot injected fuel. In particular, the *CO*
186 conversion rate deteriorates when *DT* is augmented and q_{pil} reduces, in part because of the increase in the fuel
187 autoignition delay and in part due to a reduction in the highest in-cylinder gas temperature values [4]. However, it is
188 worth observing that the engine-out *HC* and *CO* emissions do not generally represent a major critical issue at medium
189 load and speed engine conditions, even for low temperature combustion systems, since the greatest number of
190 overmixing zones and the lowest in-cylinder temperatures are present at light loads and low speeds [8]. In particular, the
191 engine-out *HC* and *CO* emission levels shown in Figs. 3 and 4 can easily be controlled by means of the diesel oxidation
192 catalyst.

193 **3.1 Nitrogen oxide and soot emissions**

194 The most critical engine-out emissions at medium load and speed engine conditions are the NO_x and soot emissions.
195 Fig. 5 shows that the engine-out NO_x emissions tend to reduce in the presence of high *EGR* rates, when either *DT*
196 increases significantly or ET_{pil} diminishes considerably, and there is no discrepancy between these general trends and
197 those obtained from conventional combustion systems. In particular, as can be inferred from the in-cylinder NO_x
198 crankshaft angle distributions shown in Figs. 9, the augment in the NO_x emissions, when ET_{pil} increases from 160 μs to
199 210 μs at DT=1200 μs, is primarily caused by the increased contribution of the NO_x emissions produced during pilot
200 combustion. This contribution to the NO_x emissions is greater than the decrease that is generated during the main
201 combustion event, because of the shortened ignition delay of the main injected fuel (cf. cases ET_{pil}=210 μs and
202 ET_{pil}=160 μs for DT=1200 μs in Fig. 8).
203 A comparison between the data given in Figs. 1 and 5 shows that there is trade-off between NO_x and *bsfc* with respect to
204 both ET_{pil} and *DT*. In fact, the combustion mode of the engine at *bmep*=5 bar is similar to that of a conventional diesel
205 engine (pure PCCI usually works for low loads and the engine tends to switch from PCCI combustion to normal
206 combustion as the load increases) and therefore the usual trade-offs of the standard diesel engine (NO_x vs. *bsfc* and also

207 NO_x vs. soot, cf. Figs. 5 and 6) can be observed. However, the NO_x emissions in Fig. 5 show very low levels and
208 reduced sensitivity to *DT* and ET_{pil}, compared to conventional combustion systems that work under moderate *EGR* rates
209 and with more advanced SOI_{main}. The applied low-temperature combustion strategy in fact employs high *EGR* rates,
210 SOI_{main} around *TDC,* as well as a reduced compression ratio. All of these features contribute to the containment of the
211 burned gas temperatures and thus improve NO_x emissions to a great extent. As a consequence, the sensitivity of NO_x to
212 the pilot injection parameters is less significant.
213 The trend of the engine-out soot emissions, with respect to $ET_{pil,}$ shown in Fig. 6, is also in line with the results that are
214 usually found in the literature for conventional diesel combustion systems: the higher the pilot injected quantity, the
215 higher the soot production. On the other hand, as can be seen in Fig. 6, the soot monotonically increases with the dwell
216 time within the 400 μs<*DT*<1200 μs range, whereas a decrease in the soot, with respect to *DT,* is usually observed for
217 moderate *EGR* rates [34]. Furthermore, the increasing trend of the soot emissions, with respect to *DT,* is more
218 pronounced as ET_{pil} increases from 160 μs to 210 μs. Similar results on the dependence of soot emissions on increasing
219 *DT* have recently been obtained in [14] for higher X_{EGR} values than 50% at low load and speed conditions, but in that
220 case the soot was shown to reduce with the pilot injected quantity at fixed *DT*, whereas this cannot be observed in
221 Fig. 6.
222 Figure 10 reports the soot emission crankshaft angle based in-cylinder distributions for the same combinations of the
223 ET_{pil} and *DT* values shown in Fig. 9. The augment in ET_{pil} at *DT*=1200 μs determines a significant increase in the soot
224 production rate during the main combustion, and this result is in line with those of conventional combustion systems.
225 As far as the effect of *DT* is concerned, the soot production rate is significantly higher at *DT*=1200 μs than at *DT*=400
226 μs for the ET_{pil}=210 μs case. In general, the main factors responsible for an increase in the soot production rate are: the
227 higher temperature of the gases during the soot growth phase, the presence of local zones with poor mixing of the fuel
228 with air, and direct interference between the hot flames of the pilot injection and the main injection. Fig. 11 shows that
229 the maximum burned gas temperatures during the main injection and combustion events are similar for the *DT*=400 μs
230 and *DT*=1200 μs cases at ET_{pil}=210 μs (the maximum values are around 2280 K, that is, higher than the typical limit of
231 about 2225 K of the pure PCCI working mode at lower loads [28]). In fact, as can be seen in Fig. 10, the soot oxidation
232 rates, which depend on the burned gas temperature values, are almost the same for the two cases. Therefore, the burned
233 gas temperature cannot be responsible for the differences that occur in the soot production rates between the *DT*=400 μs
234 and *DT*=1200 μs working conditions. Furthermore, the *HRR* trace in Fig. 8 shows that pilot combustion occurs
235 simultaneously with the main injection in the *DT*=400 μs case, whereas this does not happen for *DT*=1200 μs.
236 Therefore, no interference takes place between the hot flames of the pilot combustion and the main injection at

237 *DT*=1200 μs. In addition, since soot production is higher for the *DT*=1200 μs case, no impingement of the main
238 injection on the pilot hot flames is feasible for *DT*=400 μs, because such a remarkable interference would have a
239 dramatic effect on the soot production at *DT*=400 μs. In fact, the concomitance of the pilot combustion *HRR* and the
240 main injected flow-rate is a necessary but not sufficient condition to prove the impingement of the main injected fuel on
241 the pilot flames. Finally, the closer proximity of the pilot shot to the main injection for the *DT*=400 μs case could, in
242 principle, decrease the mean oxygen concentration around the nozzle at the start of the main injection, but even this
243 would not justify the higher soot level observed in Fig. 10 for *DT*=1200 μs, or the more general tendency of the soot
244 shown in Fig.6, which increases as *DT* grows.
245 Figure 12 reports the engine-out soot emissions as a function of the swirl actuator position (*Sw*) at 2000x5, for *DT*=1200
246 μs and ET_{pil}=190 μs (the higher the swirl actuator position, expressed as a percentage of the closure of the swirl valve,
247 the higher the swirl ratio). An oscillating pattern of the soot emissions, with respect to *Sw,* can be observed; in
248 particular, a significant augment in the soot emissions can be observed when *Sw* passes from 40% to 50%, whereas the
249 soot decreases for an increasing swirl actuator position for lower *Sw* values than 40% or higher *Sw* values than 50%. On
250 one hand, the soot should reduce monotonically as the value of the swirl ratio increases because turbulence improves
251 the air-fuel mixing. On the other hand, when the swirl ratio is changed under a fixed *DT*, local inhomogeneity of the
252 composition can occur within the cylinder, due to the interference between the burned gas clouds of the pilot
253 combustion and the main injection fuel spray. The burned gas spots, which originate from pilot combustion, rotate, due
254 to the swirl motion, and the fuel plumes, which are injected through the 7 injection holes during the main injection, can
255 impinge on them. When *DT* is fixed, a change in *Sw* modifies the rotational velocity of the pilot combustion burned
256 gases, and this alters their possible direct interaction with the main injection fuel spray, thus producing the oscillating
257 behaviour of the soot emissions, with respect to *Sw,* that can be observed in Fig. 12. The main cause of the increase in
258 the soot emissions, with respect to *DT,* could therefore be ascribed to the interaction between the burned gas clouds
259 pertaining to the pilot combustion and the main injection fuel plumes. The *DT* sweeps, the results of which are plotted
260 in Figs. 1-11, refer to *Sw*≈41%; the interference between the burned gases and the main injected fuel could be relatively
261 high at *DT*=1200 μs, ET_{pil} = 190 μs and *Sw*=41% and it could increase when either *DT* reduces from 1200 μs to 1000 μs
262 at fixed *Sw*=41% and ET_{pil} = 190 μs (cf. Fig. 6) or *Sw* rises from 41% to 50% at fixed *DT*=1200 μs and ET_{pil} = 190 μs
263 (cf. Fig. 12). A higher *Sw* implies that a smaller time interval is required for the burned gas clouds to cover a certain
264 rotation angle, whereas a lower *DT* leads to a reduced time interval between the pilot and main injection events. As a
265 consequence, in order to reach the same effect on the degree of interference between the pilot combustion burned gas
266 clouds and the fuel plumes pertaining to the main injection, either the rotational motion of the burned gas clouds

originating from the pilot combustion need to be accelerated or the *DT* needs to be reduced. Engine-out soot emissions decrease as the swirl actuation position increases beyond 50% by increasing as the *Sw* value increases, and the same result is reached when *DT* is progressively reduced below 1000 μs. In conclusion, the soot emission trends shown in Figs. 6 and 12 are both consistent with the proposed physical explanation.

The remarkable interaction phenomena between pilot combustion and the main injection, which leads to increased soot emissions, were investigated and described by means of numerical simulations in [17], even though, in that case, the fuel plumes of the main injection impinged directly on the pilot hot flames and the situation was therefore more critical. It is worth observing that the presence, in the burning zones of the main injected fuel, of relatively high equivalent ratios, which are induced by the increasing interference between the pilot combustion burned gas clouds and the main injection fuel plumes as *DT* grows, can concur to determine the slight decrease in the NO_x emissions with respect to *DT* which is observed in Fig. 5 (NO_x are only produced for smaller local ϕ than 1.5). In other words, the proposed explanation for the increase in the soot emissions with respect to *DT* is also consistent with the NO_x emission results given in Fig. 5.

Figures 13 and 14 report NO_x and soot as functions of *DT* for ET_{pil}=170 μs, ET_{pil}=200 μs and ET_{pil}=230 μs in the *bmep*=8 bar and *n*=2500 rpm case. Table 3 reports the values of the most important engine parameters, which were maintained constant during the considered *DT* sweeps (the *MFB50* variations were within 1°CA). The NO_x and soot trends, with respect to both *DT* and ET_{pil}, generally confirm those at *bmep*=5 bar and *n*=2000 rpm. The NO_x emissions are very low for the considered working condition, and the presence of a weak trade-off between NO_x and soot is observed with respect to *DT*. Furthermore, the soot generally increases with *DT* and this behaviour can still be attributed to inhomogeneity in the combustion chamber, with the presence of spots of burned gases derived from the pilot combustion event, which interfere with the main injection fuel spray. The pattern of the engine-out soot emissions, with respect to the swirl ratio, was verified to be oscillating for the ET_{pil}=230 μs case, and complete consistency was again found between this soot versus the *Sw* diagram and the corresponding *DT* sweep pattern in Fig. 14.

4. RATE-SHAPED MAIN INJECTIONS BY MEANS OF INJECTION FUSION IN SOLENOID COMMON RAIL INJECTORS

An innovative type of injection schedule is represented in Fig. 15, with reference to an experimental test performed at the hydraulic test rig with the same solenoid Common Rail injectors installed on the engine. When the pilot injection is sufficiently close to the main shot, the electrical current signal related to ET_{main} starts before the needle has closed the nozzle during the pilot-injection, which, in these conditions, is referred to as pre-injection. As a consequence, injection fusion occurs [39], and the pre and main shots give rise to a rate-shaped single injection event. When an additional pilot

297 shot is added before the pre and main joined injections, this fusion strategy is here referred to as *pmM*, whereas the
298 simple pilot-main strategy, the effects of which were analyzed in the previous section, is indicated with the *pM*
299 acronym.
300 The fusion of the pre and main shots reproduces a pattern that is similar to that of boot shaped main injections, which
301 are typical of direct-acting piezoelectric injectors [41], even though the injection fusion strategy applied to the solenoid
302 injectors leads to less flexibility. Boot injection is usually performed in the medium-to-high load zone of the *NEDC* area
303 of conventional combustion systems in order to reduce the amount of fuel that is mixed with air during the early
304 injection process. The autoignition of premixed fuel and air is therefore greatly reduced [42] and, as a consequence, the
305 maximum rates of heat release are limited, thus determining combustion noise reductions of up to 3-4 dBA [11, 43].
306 Furthermore, boot injection usually induces a remarkable reduction in engine-out NO_x emissions, without a huge
307 detriment to soot formation and fuel consumption in most cases [44, 45].
308 The innovative rate-shaped injection that is shown in Fig. 15 has been applied in an attempt to achieve similar benefits
309 in solenoid injectors to those resulting from the application of boot shaped injection profiles in piezoelectric injectors.
310 Table 4 reports the engine conditions under which the DT_{pil} sweeps have been performed for a *pmM* injection schedule;
311 DT_{pre} has been fixed at 100 μs in order to guarantee the presence of injection fusion events between the pre and main
312 shots in all of the examined working conditions. The ET_{pil} value is equal to 205 μs at 1500x5 (q_{pil}≈2 mm^3), while
313 ET_{pil}=180 μs at 2000x5 and ET_{pil}=166 μs at 2500x8 (q_{pil}≈1 mm^3 in both cases). Furthermore, SOI_{main} and ET_{main} have
314 been adjusted during each DT_{pil} sweep in order to maintain the same *MFB50*, which is reported in Table 4, and the same
315 *bmep*, respectively.

316 5. EFFECT OF THE PILOT SHOT ON RATE-SHAPED MAIN INJECTIONS AND LOW-
317 TEMPERATURE COMBUSTION

318 Figure 16 reports *CN* as a function of DT_{pil} for the engine points considered in Table 4. As can be inferred, the effects of
319 DT_{pil} on *CN* continue to be almost the same as in Fig. 2 for the 2000x5 and 2500x8 cases. In particular, the combustion
320 noise reduces as DT_{pil} increases in the 400 μs≤ DT_{pil} ≤1600 μs range for 2000x5 and 2500x8, whereas it remains almost
321 constant as DT_{pil} varies for 1500x5. The *CN* levels for 2000x5 shown in Fig. 16 are generally 2-3 dBA lower than the
322 ones reported in Fig. 2 for a similar ET_{pil} value. Furthermore, almost the same difference can be observed between the
323 *CN* data for *pmM*, plotted with filled round symbols in Fig. 16, and the corresponding data at 2500x8 for the standard
324 pilot-main (*pM*) injection schedule with similar ET_{pil} (cf. data with empty circle symbols). These reductions in the *CN*
325 levels, compared to the *pM* strategy, can be ascribed to the rate-shaped main injection. However, the benefits of this
326 feature are slightly underestimated in the comparisons, since the ET_{pil} of the *pM* strategy is always slightly higher than

the corresponding value pertaining to the *pmM* strategy (the higher the ET_{pil} in Fig.2, the lower the *CN*). Furthermore, the presence of the rate-shaped main injection makes the impact of DT_{pil} on the combustion noise marginal, as can be seen in Fig. 16, since the variations in *CN* with DT_{pil} are lower than 1 dBA along each DT_{pil} sweep that has been considered.

Figure 17 shows that *bsfc* generally remains almost constant when passing from DT_{pil}=400 μs to DT_{pil}=1600 μs for the three considered engine points tested with the *pmM* strategy. However, the values of *bsfc* for *pmM* at 2000x5 are roughly 2-3% higher than those for ET_{pil}=190 μs shown in Fig. 1 (*pM* strategy), although the penalty estimation should take into account that, in Fig.17, ET_{pil}=180 μs instead of 190 μs and that, in Fig. 1, *bsfc* tends to increase when ET_{pil} reduces. This means that 2-3% is probably an overestimation of the *bsfc* penalty due to injection fusion. In fact, the deterioration of *bsfc* at 2500x8 for the *pmM* strategy, compared to the *pM* injection schedule (cf. data with empty circle symbols in Fig. 17), is less than 1% for almost the same ET_{pil}.

The general slight deterioration of *bsfc* for the *pmM* strategy, compared to the *pM* schedule, is a consequence of the lengthening of the overall injection event, due to the rate-shaped main injection. The (EOI_{main}–SOI_{pil}) angular intervals that correspond to a certain DT_{pil} in the *pmM* strategies at 2000x5 and 2500x8 have in fact been verified to generally be slightly higher than the corresponding values, measured under the same dwell time, in the *pM* cases at 2000x5 and 2500x8, respectively. Furthermore, *MFB50* is about 1.5°CA higher at 2000x5 for the *pmM* calibration than for the *pM* one, and a delayed combustion on its own makes *bsfc* worse (the differences in *MFB50* between the two strategies are instead lower than 0.7°CA at 2500x8). All these circumstances explain the general slight increase in *bsfc* that occurs for the *pmM* injection schedule at the examined working conditions.

Finally, the trends of the engine-out *CO* and *HC* emissions with respect to DT_{pil} have been verified to be the same for the *pmM* calibration as those shown in Figs. 3 and 4 for the *pM* calibration, that is, the *HC* and *CO* emissions increase with respect to DT_{pil} in the 400 μs <DT_{pil}<1500 μs range. Furthermore, the levels of these emissions for the *pmM* strategy at 2000x 5 and 2500x8 are almost the same as those for the *pM* strategy applied at the same key points and for similar ET_{pil} values.

5.1 Nitrogen oxide and soot emissions

The soot emissions shown in Fig. 18 are generally higher than the corresponding ones shown in Fig. 6 (ET_{pil}=190 μs case) and Fig. 14 (ET_{pil}=170 μs case). Furthermore, as can be observed in Fig. 18, the soot generally tends to reduce as DT_{pil} is increased for the 2000x5 and 2500x8 engine working conditions, and these trends are not in line with those shown in Figs. 6 and 14 for the *pM* strategy.

Figures 19-21 report the in-cylinder analyses, conducted at DT_{pil}=400 μs, DT_{pil}=1000 μs and DT_{pil}=1500 μs, for the 2000x5 key point and the *pmM* injection schedule. The soot production rate is maximum and minimum at~~t~~ DT_{pil}=400 μs and DT_{pil}=1500 μs, respectively, whereas it shows an intermediate value at DT_{pil}=1000 μs (cf. Fig. 21). The burned gas temperatures reach the highest values earlier as DT_{pil} increases (cf. Fig. 20), and the rate of the *HRR* rise during the main combustion is minimum for the DT_{pil}=400 μs case (cf. Fig. 19). If the pilot shot is closer to the main injection, the mean oxygen concentration decreases in a zone around the nozzle at the start of the main injection, and this could explain the lower $d(HRR)/d\theta$ values in the $365°CA<\theta<375°CA$ interval for the DT_{pil}=400 μs case. The decrease in the mean oxygen concentration around the nozzle, as DT_{pil} reduces, tends to increase the soot production to $\theta\approx376°CA$, and this result is in agreement with the data shown in Fig. 18. Finally, there is no simultaneity between the *HRR* trace pertaining to the pilot combustion and the injection rate for the DT_{pil}=1000 μs and DT_{pil}=1500 μs conditions in Fig 19, whereas some concomitance could be ~~is~~ present in the DT_{pil}=400 μs case. However, the soot deteriorates in almost the same way in Fig. 18, when DT_{pil} is reduced from DT_{pil}=1500 μs to DT_{pil}=1000 μs and then from DT_{pil}=1000 μs to DT_{pil}=400 μs at 2000x5. This seems to suggest that the main injection does not impinge on the pilot flames in the DT_{pil}=400 μs case.

Figure 22 reports the soot emissions as a function of *Sw* for the 1500x5, 2000x5 and 2500x8 engine points; DT_{pre}=100 μs in all of the cases, while DT_{pil}=400 μs for 1500x5, DT_{pil}=1590 μs for 2000x5 and DT_{pil}=1550 μs for 2500x8. As can be inferred, oscillating behaviour of the soot emissions occurs, with respect to *Sw,* for the 2000x5 and 2500x8 cases, while the soot emissions decrease monotonically, with respect to *Sw,* for the 1500x5 engine point. This means that an appreciable interference between the pilot injection burned gas clouds and the main injection fuel plumes is likely to occur in the tests at 2000x5 and 2500x8, and this phenomenon affects the soot emissions to a great extent, whereas such an interference is probably negligible for the tests at 1500x5. In the latter case, the soot in fact decreases monotonically with respect to *Sw*, in line with the basic theories on the effects of the swirl-ratio on particulate matter. Furthermore, the soot values at 1500x5 shown in Fig. 18 are significantly lower than those at 2000x5, probably in part due to the absence of the impingement of the main injected fuel on the burned gases of the pilot combustion. On the other hand, the augment in the maximum values of soot emission at 2500x8, compared to the maximum values at 1500x5 and 2000x5, is also due to the increased *bmep* value.

In Figs. 16-21, with reference to the *pmM* strategy, the swirl actuator position is equal to 40% for the tests at 2000x5, while *Sw*=45% for the tests at 1500x5 and *Sw*=35% for those at 2500x8, as indicated in Table 4. The *Sw* values, which are used in the DT_{pil} sweeps at 2000x5 and 2500x8, refer to the minimum soot values of the swirl sweep diagrams in Fig. 22. The soot emissions increase when *Sw* passes from 40% to 60% at 2000x5 or from 35% to 55% at 2500x8. On

386 the other hand, the soot emissions are shown to increase in Fig. 18, when DT_{pil} diminishes from 1500 μs to 400 μs at
387 2000x5 or when DT_{pil} diminishes from 1500 μs to 500 μs at 2500x8. Furthermore, the soot again decreases at 2500x8
388 for Sw>55% in Fig. 22 and for DT_{pil}<500 μs in Fig. 18.
389 The trends of the soot for the 2000x5 and 2500x8 working conditions, with respect to DT_{pil} in Fig. 18, are therefore
390 consistent with those of the soot with respect to Sw in Fig. 22, if impingement of the fuel plumes of the main injection
391 on the burned gases of the pilot combustion occurs. When reference is made to Sw=40% and DT_{pil}= 1590 μs at 2000x5
392 or to Sw=35% and DT_{pil} = 1550 μs at 2500x8, either an increase in Sw (burned gas rotates more quickly) or a decrease
393 in DT_{pil} (pilot injection occurs closer to the main injection) could lead to a more intense interference between the pilot
394 combustion burned gases and the main injected fuel, thus increasing the soot emissions.
395 Figure 23 reports the engine-out NO_x emissions versus DT_{pil} for 1500x5, 2000x5 and 2500x8. The influence of DT_{pil} is
396 marginal, and is even weaker than the influence of DT in Figs. 5 and 13; the in-cylinder analyses on NO_x emissions
397 conducted at 2000x5 in Fig. 24 show a slight improvement in the DT_{pil}=400 μs case. In general, the NO_x emission
398 levels in Fig. 23 do not change significantly compared to those of the *pM* strategy (cf. Figs. 5 and 13). NO_x emissions
399 are mainly produced in diesel engines because of the high local temperatures, and the introduction of the rate-shaped
400 main injection is in fact aimed at lowering the maximum burned gas temperature. Nevertheless, the presence of low
401 temperature combustion, featuring high *EGR* rates and postponed *MFB50*, applied to a low-compression ratio engine
402 (each of these features induces a diminution in the maximum burned gas temperature), and the reduced time interval of
403 the initial phase of the main injection during which the needle lift remains stationary at partial lift (the injection scheme
404 in Fig. 15 leads to poor flexibility in the management of the flow-rate shaping), seem to make the benefits of the rate-
405 shaped main injection on the engine-out NO_x emissions ineffective. The improvement that occurs for the DT_{pil}=400 μs
406 case (Fig. 24) could be due to the higher local equivalence ratios in the main combustion zone, caused by the
407 interference of the main injected fuel with the pilot combustion burned gases.

408 ## 6. CONCLUSIONS.

409 An experimental investigation has been carried out at a dynamometer cell on a low-compression ratio diesel engine,
410 fueled with diesel oil and managed through the adoption of a low-temperature combustion strategy, in order to assess
411 the influence of pilot injection on engine-out pollutant emissions and performance. The tests have been conducted at
412 medium load and engine speed conditions by implementing a *pM* injection schedule characterized by the presence of
413 high *EGR* rates and postponed SOI_{Main} angles, according to a late partial PCCI strategy.
414 The benefits of an innovative *pmM* strategy featuring a rate-shaped main injection, which was obtained by designing an
415 injection fusion event between a so-called pre injection (performed after the pilot shot) and a main injection, have been

investigated for the considered low-temperature combustion engine. The proposed injection rate shaping technique should represent the response of the solenoid injector technology to the boot injection that is used in piezoelectric injectors.

The main achievements of the experimental activity, which were interpreted with the support of a three zone combustion diagnostic tool, are outlined in a synoptic way as follows:

- for the *pM* strategy, the dependence of the engine-out emissions, combustion noise and brake specific fuel consumption on the dwell time and injected quantity of the pilot injection is generally in line with the results of conventional combustion systems. *HC* and *CO* emissions increase as *DT* grows and decrease for increasing q_{Pil}; the same trends are generally observed for brake specific fuel consumption. The combustion noise also reduces as q_{Pil} grows, but the dependence of *CN* on *DT* is the opposite to the dependence which is usually observed in conventional combustion systems, that is, *CN* has been found to reduce for increasing *DT* values. This discrepancy has been proved to be related to the delayed SOI_{main} angles, which induce a higher peak value of *HRR* for the main injection premixed combustion as *DT* reduces at fixed ET_{pil}, and thus determine a monotonically decreasing trend of *CN* with respect to *DT*. Finally, NO_x emissions increase when q_{pil} grows and slightly-decrease as *DT* is enlarged;
- ET_{pil} should be increased for the *pM* strategy in order to reduce *CN*, *HC*, CO and *bsfc*. The engine-out NO_x emissions generally take on low values, due to the low temperature combustion strategy;
- the *pmM* strategy leads to an improvement in combustion noise, compared to the *pM* strategy, but also to a deterioration of both the soot emissions and the brake specific fuel consumption. These outcomes are in line with the results on boot-shaped injection profiles in diesel engines fueled with piezoelectric injectors. However, no benefits of the *pmM* strategy have been found for the NO_x emissions, as usually occurs for boot injection in conventional combustion systems;
- the engine-out NO_x emissions generally show reduced sensitivity to the pilot injection *DT* and do not improve when rate-shaped main injections, realized by means of injection fusion, are implemented. This can be ascribed to the low-compression ratio diesel engine that was used, which was managed with a low-temperature combustion strategy and employed postponed SOI_{Main} and high *EGR* rates. Each of these engine design characteristics generates a reduction in NO_x emissions, which become less sensitive to the adopted multiple injection strategy;
- the soot emissions decreased for both the *pM* and *pmM* strategies, when q_{pil} was reduced, but all of the other parameters were kept fixed. The dependence of the soot emissions on pilot injection timing generally seems to depend on a fluid dynamics interference between pilot combustion and the main (or pre-main) injected fuel. The burned gas clouds that originate from the pilot combustion rotate, due to the swirl motion, and the fuel plumes, which are injected through the injection holes during the main injection, can impinge on them. When the dwell time is varied, the degree of

intensity of this interference between the burned gas spots and the main injection is altered, and this determines a change in the soot emissions, which can either become worse or improve with the variations in the pilot injection timing;

- a coupled analysis of the dependence of soot emissions on dwell time and *Sw* is recommended in order to obtain a better understanding of the reasons behind soot production, especially in the presence of high *EGR* rates. When the soot emissions decrease monotonically with respect to *Sw*, no remarkable interference phenomena occur between the burned gases of the pilot combustion and the main (or pre-main) injected fuel hot flames (this was the situation at the 1500x5 engine point). On the other hand, if soot emission oscillations are detected with respect to *Sw* (these were verified to exist at the 2000x5 and 2500x8 engine points), the main injected fuel impinges on either the hot flames or on the burned gases of the pilot combustion, and the intensity of this fluid dynamical interference changes when the pilot injection timing or *Sw* is changed. The dependence of soot emissions on dwell time is always physically consistent with the dependence of soot emissions on swirl ratio, if interference between the main injected fuel and burned gases from the pilot combustion is assumed.

7. NOMENCLATURE.

bmep	brake mean effective pressure
bsfc	brake specific fuel consumption
CA	crank angle (degree)
CN	combustion noise
DT	dwell time between the pilot and main injection shot
DT_{Pil}	dwell time between the pilot and pre injection shots
DT_{Pre}	dwell time between the pre and main injection shots
ECU	electronic control unit
EGR	exhaust gas recirculation
EOI_{Main}	electrical end of the electrical command for the main injection
HC	unburned hydrocarbons
HRR	heat release rate
$\dot{m}_a$	fresh-air mass flow-rate
$\dot{m}_{EGR}$	exhaust gas mass flow-rate
MFB50	angle at which 50% of the combustion mixture has burned
n	engine speed

477	*NEDC*	New European Driving Cycle
478	NO_x	nitrogen oxides
479	*PCCI*	Premixed Charge Compression Ignition
480	p_{cyl}	in-cylinder pressure
481	*pm*	pilot and main injection strategy
482	*pmM*	pilot and pre-main injection strategy (with injection fusion)
483	p_{rail}	nominal rail pressure level
484	q_{Pil1}	volume of fuel injected in the pilot injection
485	SOI_{Main}	electrical start of the main injection
486	SOI_{Pil}	electrical start of the pilot injection
487	*Sw*	swirl actuator position
488	T_b	burned gas temperature
489	*TDC*	top dead center
490	X_{EGR}	mass fraction of exhaust gas recirculation
491	ε	engine compression ratio
492	ϕ	equivalence ratio
493	θ	crankshaft angle in the simulations

494 8. REFERENCES.

495 [1] Heywood, J. B., 1988, “Internal combustion engine fundamentals”, McGraw Hill, New York.

496 [2] Maiboom, A., Tauzia, X., and Hetet, J. F., 2008, “Experimental study of various effects of exhaust gas
497 recirculation on combustion and emissions of an automotive direct injection diesel engine”, *Energy*, 33,
498 pp. 22-34.

499 [3] Ehleskog, R., Ochoterena, R. L., and Andersson., S., 2007, “Effects of multiple injections on engine-out
500 emission levels including particulate mass from an HSDI diesel engine”, SAE paper. 2007-01-0910.

501 [4] Suh, K. H., 2014, “Study on the twin-pilot-injection strategies for the reduction in the exhaust emissions
502 in a ow-compression engine”, *Proc. IMechE Part D: J. of Automobile Engineering*, vol. 228(3), pp. 335-343.

503 [5] Han, Z., Uludogan, A., Hampson, G. J., and Reitz, R. D., 1996, “Mechanism of soot and NO_x emission
504 reduction using multiple-injection in diesel engine”, SAE paper 960633.

505 [6] Yun, H. H., Sellnau, M., Milovanovic, N., and Zuelch, S., 2008, "Development of premixed low-
506 temperature diesel combustion in a HSDI engine", SAE paper no. 2008-01-0639.
507 [7] Helmantel, A., and Golovitchev, 2009, "Injection strategy optimization for a light duty DI diesel engine
508 in medium load conditions with high EGR rates", SAE paper no. 2009-01-1441.
509 [8] d'Ambrosio, S., and Ferrari, A., 2015, "Potential of double pilot injection strategies optimized with the
510 design of experiments procedure to improve diesel engine emissions and performance", *Applied Energy*,
511 volume 155, p. 918-932.
512 [9] Ferrari, A., and Mittica, A., 2015, "Response of different injector typologies to dwell time variations and
513 hydraulic analysis of digital and continuous rate shaping injection schedules for the improvement of engine-
514 out emissions, fuel consumption and noise", submitted to *Applied Energy*.
515 [10] Nishimura, T., Satoh, K., Takahashi, S., and Yokota, K., 1998, "Effects of fuel injection rate on
516 combustion and emission in a DI diesel engine", SAE paper 981929.
517 [11] Kastner, O., Atzler, F., Juvenelle, C., Rotondi, R., and Weigand, A., 2009, "Directly actuated piezo
518 injector for advanced injection strategies towards cleaner diesel engines" Towards Clean Diesel Engines,
519 TCDE 2009.
520 [12] Predelli, O., Gratzke, R., Sommer, A., Marohn, R., Atzler, F., Schule, H., Kastner, O., and Nozeran, N.,
521 2010, "Continuous injection-rate shaping for passenger-car diesel engines – Potential, limits and feasibility",
522 31st International Vienna Engine Symposium.
523 [13] Payri, F., Broatch, A., Salavert, J. M., Martín, J., 2010, "Investigation of Diesel combustion using
524 multiple injection strategies for idling after cold start of passenger-car engines", *Experimental Thermal and*
525 *Fluid Science*, 34, pp. 857–865.
526 [14] Lee, J. W., Choi, S. M., Yu, S., Choi, H., and Min, K. D., 2013, "Comparison of the effects of multiple
527 injection strategy on the emissions between moderate and heavy EGR rate conditions: part 1-pilot
528 injections", *Journal of Mechanical Science and Technology*, 27(4), pp. 1135-1141.
529 [15] Tullis, S., and Greeves, G., 1996, " Improving NO_x versus bsfc with EUI 200 using EGR and pilot
530 injection for heavy duty diesel engines", SAE paper No. 960843.

[16] Bhatt, N. M., Rathod, P. P., Sorathiya, A. S., and Patel, R., 2013, "Effect of the multiple injection on the performance and emission of diesel engine. A review study", *International Journal of Emerging Technology and Advanced Technology*, vol. 3 (3).

[17] Busch, S., Zha, K. and Miles, P.C., 2014, "Investigations of closely coupled pilot and main injections as a mean to reduce combustion noise", 8th Thiesel Conference, Valencia 9th-12th September.

[18] Badami, M., Mallamo, F., Millo, F., and Rossi, E. E., 2003, "Experimental investigation on the effect of multiple injection strategies on emissions, noise and brake specific fuel consumption of an automotive direct injection common-rail diesel engine", *International journal of engine research* 4(4), pp. 299-314.

[19] O' Connor, J., and Musculus, M., 2013, "Post Injections for Soot Reduction in Diesel Engines: A Review of Current Understanding," *SAE Int. J. Engines* 6(1), pp. 400-421.

[20] Mobasheri, R. Peng, Z., 2012, "Investigation of pilot and multiple injection parameters on mixture formation and combustion characteristics in a heavy duty DI-diesel engine", SAE paper 2012-04-16.

[21] Park, C., Kook, S., and Bae, C., 2004, "Effects of multiple injections in a HSDI diesel engine equipped with Common Rail injection system", SAE paper no. 2004-01-0127.

[22] Carlucci, A. P., Ficarella, A., and Laforgia, D., 2006, "Control of the combustion behavior in a diesel engine using early injection ad gas addition", *Applied Thermal Engineering*, 26, pp. 2279-2286.

[23] Okude, K., Mori, K., Shiino, S., Yamada, K., and Matsumoto, Y., 2007, "Effects of multiple injections on diesel emissions and combustion characteristics", SAE paper no. 2007-01-4178.

[24] Lee, J., Jeon, J., Park, J., and Bae, C., 2009, "Effect of multiple injection strategies on emission and combustion characteristics in a single cylinder direct-injection optical engine", SAE paper no. 2009-01-1354.

[25] Fang, Q., Fang, J., Zhuang, J., and Huang, Z., 2012, "Influences of pilot injection and exhaust gas recirculation (EGR) on combustion and emissions in a HCCI-DI combustion engine", *Applied Thermal Engineering*, 48, pp. 97-104.

[26] Das, P., Subbarao, P.M.V., and Subrahmanyam, J. P., 2015, "Effect of main injection timing for controlling the combustion phasing of a homogeneous charge compression ignition engine using a new dual injection strategy", *Energy Conversion and management*, 95, pp. 248-258.

557 [27] Yu, W., Yang, W., Mohan, B., Tay, K., Zhao, F., and Chou, S. K., 2015, "Multiple injections study
558 based on an advanced combustion investigation system", 7th International Conference on Applied Energy-
559 ICAE2015, *Energy Procedia*, 75, pp. 900-905.
560 [28] Imtenan, S., Varman, M., Masjuki, H. H., Kalam, M. A., Sajjad, H. , Arbab, M. I., and Rizwanul Fattah,
561 I. M., 2014, "Impact of low temperature combustion attaining strategies on diesel engine emissions for diesel
562 and biodiesels: A review", *Energy conversion and management*, 80, pp. 329-356.
563 [29] Benajes, J., Molina, S., García, A., Monsalve-Serrano, J., and Durrett, R., 2014, "Performance and
564 engine-out emissions evaluation of the double injection strategy applied to the gasoline partially premixed
565 compression ignition spark assisted combustion concept", *Applied Energy*, Volume 134, pp. 90-101.
566 [30] Lee, J., Chu, S., Cha, J., Choi, H., and Min, K., 2015, "Effect of the diesel injection strategy on the
567 combustion and emissions of propane/diesel dual fuel premixed charge compression ignition engines",
568 *Energy*, Volume 93, Part 1, pp. 1041-1052.
569 [31] Wang, Y., He, L., Zhou, L. , and Li, W., 2010, "Effects of DME pilot quantity on the performance of a
570 DME PCCI-DI engine", *Energy Conversion and Management*, Volume 51, Issue 4, pp. 648-654.
571 [32] d'Ambrosio S., Ferrari, A., and Spessa, E., 2013, "Analysis of the *EGR* System Performance in Modern
572 Diesel Engines", ASME Transactions, *Journal of Engineering for Gas Turbines and Power*, vol. 135 n. 8,
573 Art. No. 081601, pp. 1-13 - ISSN 0742-4795.
574 [33] Lee, Y., and Huh, K. Y., 2014, "Analysis of different modes of low temperature combustion by ultra-
575 high EGR and modulated kinetics in a heavy duty diesel engine", *Applied Thermal Engineering*, vol. 70 (1),
576 pp. 776-787.
577 [34] Zheng, Z., Yue, L., Liu, H., Zhu, Y., Zhong, X., and Yao, M., 2015 "Effect of two-stage injection on
578 combustion and emissions under high EGR rate on a diesel engine by fueling blends of diesel/gasoline,
579 diesel/n-butanol, diesel/gasoline/n-butanol and pure diesel", *Energy Conversion and Management*, vol. 90,
580 pp. 1-11.
581 [35] Finesso, R, and Spessa, E., 2014, "A real time zero-dimensional diagnostic model for the calculation of
582 in-cylinder temperatures, HRR and nitrogen oxides in diesel Engines". *Energy Convers Management*; 79, pp.
583 498–510.

584 [36] d'Ambrosio S. and Ferrari A., 2012, "Diesel Injector Coking: Optical-Chemical Analysis of Deposits
585 and Influence on Injected Flow-rate, Fuel Spray and Engine Performance", ASME *Transactions, Journal of*
586 *Engineering for Gas Turbines and Power*, vol. 134 n. 6, Art. No. 062801, pp. 1-14 - ISSN 0742-4795.
587 [37] d'Ambrosio, S., Finesso, R., and Spessa, E., 2011, "Calculation of mass emissions, oxygen mass
588 fraction and thermal capacity of the inducted charge in SI and diesel engines from exhaust and intake gas
589 analysis", *Fuel*, vol. 90, Issue 1, pp. 152-166.
590 [38] Baratta M., Catania A.E., Ferrari A., Finesso R. and Spessa E., 2011, "Premixed-Diffusive Multizone
591 Model for Combustion Diagnostics in Conventional and PCCI Diesel Engines", *ASME Trans*. *Journal of*
592 *Engineering for Gas Turbines and Power*, vol. 133 n. 10, Art. No. 102801, pp. 1-13.
593 [39] Catania A.E., Ferrari A. and Spessa E., 2009, "Numerical-Experimental Study and Solutions to Reduce
594 the Dwell Time Threshold for Fusion-Free Consecutive Injections in a Multijet Solenoid-Type C.R.
595 System", *ASME Trans*. *Journal of Engineering for Gas Turbines and Power*, vol. 131, Art. No. 022804, pp.
596 1-14 - ISSN 0742-4795. DOI: 10.1115/1.2938394.
597 [40] Hotta, Y., M. Inayoshi, et al., 2005, "Achieving lower exhaust emissions and better performance in a
598 HSDI diesel engine with multiple injections", SAE paper 2005-01-0928.
599 [41] Ferrari A., and Mittica, A., 2012, "FEM Modeling of the Piezoelectric Driving System in the Design of
600 Direct-Acting Diesel Injectors", *Applied Energy*, vol. 99, p. 471-483 - ISSN 0306-2619. DOI:
601 10.1016/j.apenergy.2012.05.048.
602 [42] Pajot, O., 2006. "Injection rate shaping with the TwinCR system: a coupled experimental and modelling
603 investigation", Diesel Engine 2006, May 31-June 1, 2006, Ecole Centrale de Lyon.
604 [43] Dober, G., Tullis, S., Greeves, G., Milovanovic, N., Hardy, M., and Zuelch, S., "The impact of injection
605 strategies on emissions reduction and power output of future diesel engines", 2183, SAESP; 183.
606 [44] Mohan, B., Yang, W., and Chlu, S. K., 2013, "Fuel injection strategies for performance improvement
607 and emission reduction in compression ignition engines - A review", Renewable *and Sustainable Energy*
608 *Reviews*, 28, pp. 664-676.
609 [45] Desantes, JM, Benajes, J, Molina, S, and Gonzales, CA, 2004, "The modification of the fuel injection
610 rate in heavy-duty diesel engines. Part 1: Effects on engine performance and emissions", *Applied Thermal*
611 *Engineering*, 24, pp. 2701-2714.

612 **9. TABLES AND FIGURES**

613

Engine type	2.0L Euro 5
Displacement	1956 cm^3
Bore × stroke	83.0 mm × 90.4 mm
Compression ratio	16.3
Valves per cylinder	4
Turbocharger	Twin-stage with valve actuators and WG
Fuel injection system	Common Rail 2000 bar solenoidal with 7 injection holes
Specific power and torque	71 kW/l – 205 Nm/l
EGR system type	Short-route cooled EGR

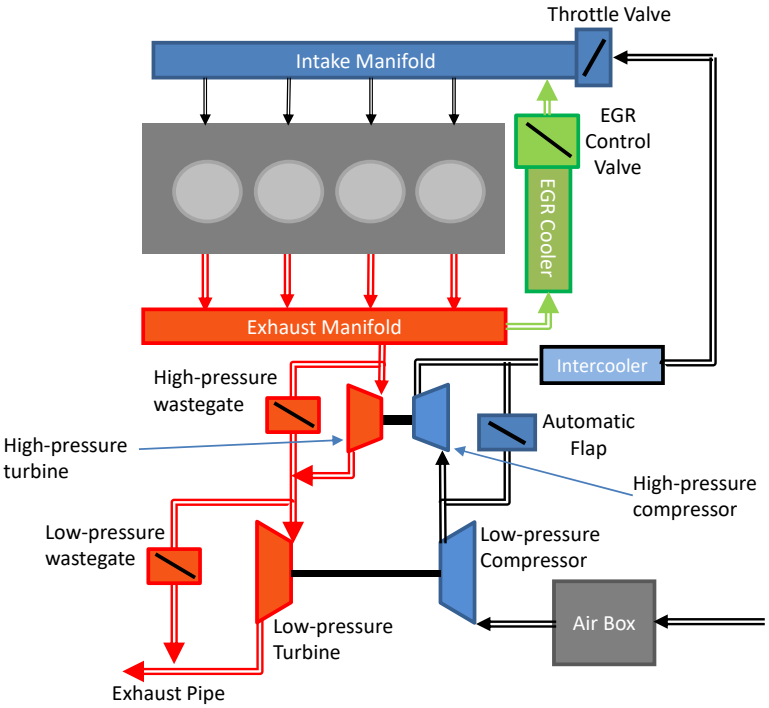

Table 1. Main specifications and schematic of the tested engine.

614

Quantity	Value
SOI_{Main} [°CA ATDC]	0.5
X_{EGR} [%]	40.7
Sw [%]	41
p_{Rail}[bar]	750
Boost [bar]	1.35
Global ϕ [-]	0.63
MFB50 [°CA ATDC]	18.0

615

Table 2: main parameters of the pilot-main calibration for the *DT* sweeps conducted at the 2000x5 engine point.

Quantity	Value
SOI_{Main} [°CA ATDC]	–3.5
X_{EGR} [%]	29.3
Sw [%]	35
p_{Rail}[bar]	1200
Boost [bar]	1.92
Global ϕ [-]	0.65
MFB50 [°CA ATDC]	17.0

Table 3: main parameters of the pilot-main calibration for the *DT* sweeps conducted at the 2500x8 engine point.

Quantity	Value at 1500x5	Value at 2000x5	Value at 2500x8
SOI_{Main} [°CA ATDC]	–0.5	3	–2.5
ET_{Pil1} [µs]	205	180	166
DT_{pre} [µs]	100	100	100
X_{EGR} [%]	41	39	29.5
Sw [%]	45	40	35
p_{Rail}[bar]	775	650	1000
Boost [bar]	1.15	1.35	1.95
Global ϕ [-]	0.67	0.63	0.63
MFB50 [°CA ATDC]	12.5	19.5	17.5

Table 4: main variables of the *pmM* calibration for the DT_{Pil} sweeps conducted at different engine points.

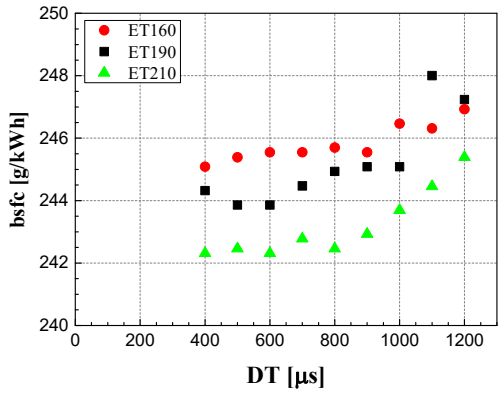

Figure 1. bsfc versus *DT* at different ET_{pil} (bmep=5 bar, n=2000 rpm).

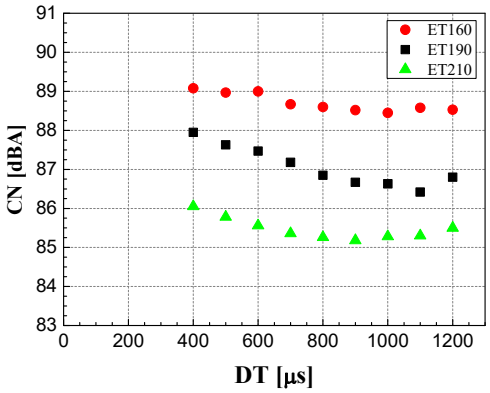

Figure 2. *CN* versus *DT* at different ET_{pil} (bmep=5 bar, n=2000 rpm).

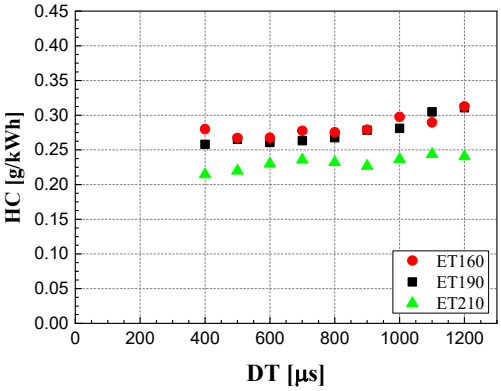

Figure 3. *HC* versus *DT* at different ET_{pil} (*bmep*=5 bar, *n*=2000 rpm).

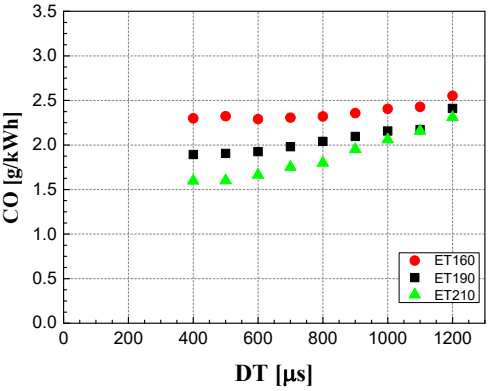

Figure 4. *CO* versus *DT* at different ET_{pil} (*bmep*=5 bar, *n*=2000 rpm).

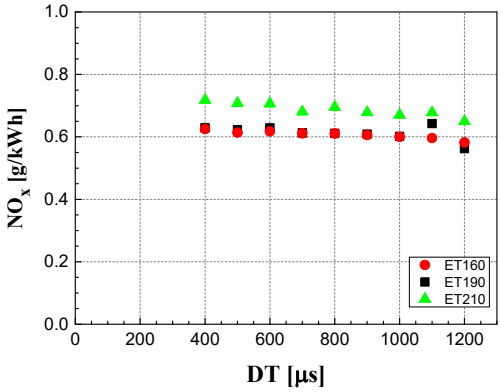

Figure 5. NO_x versus *DT* at different ET_{pil} (*bmep*=5 bar, *n*=2000 rpm).

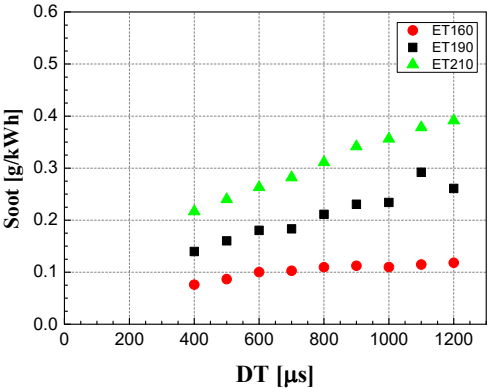

Figure 6. Soot versus *DT* at different ET_{pil} (*bmep*=5 bar, *n*=2000 rpm).

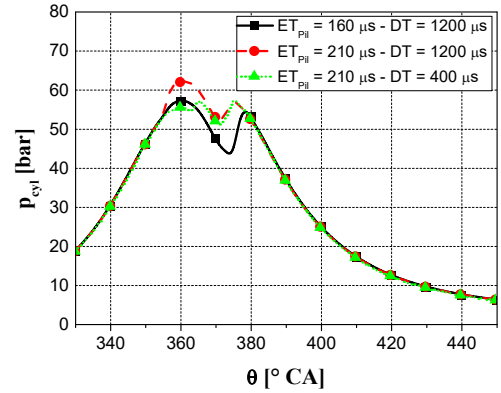

Figure 7. p_{cyl} versus θ distributions for distinct values of ET_{pil} and *DT* (*bmep*=5 bar, *n*=2000 rpm).

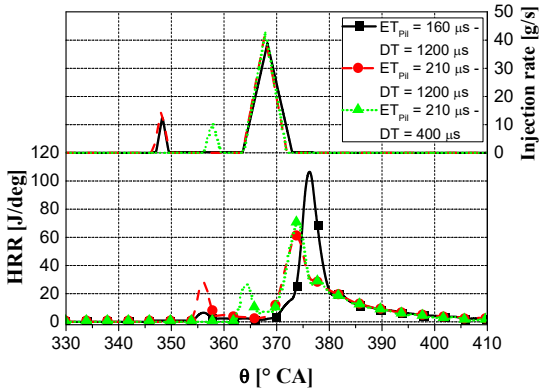

Figure 8. *HRR* and injected flow-rate versus θ traces for distinct values of ET_{pil} and *DT* (*bmep*=5 bar, *n*=2000 rpm).

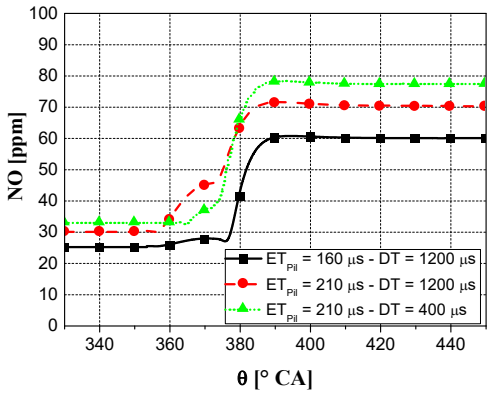

Figure 9. NO_X versus θ distributions for distinct values of ET_{pil} and DT ($bmep$=5 bar, n=2000 rpm).

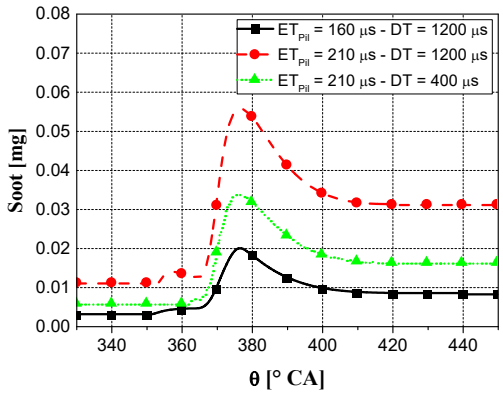

Figure 10. Soot versus θ distributions for distinct values of ET_{pil} and DT ($bmep$=5 bar, n=2000 rpm).

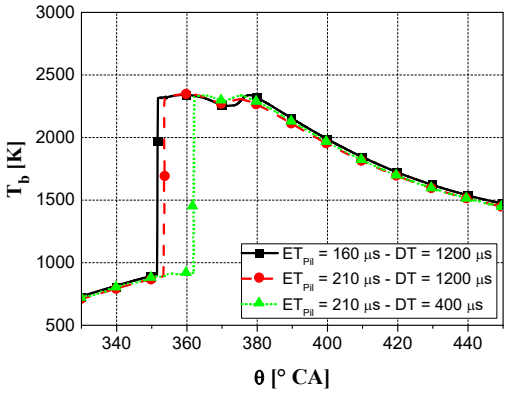

Figure 11. T_b versus θ distributions for distinct values of ET_{pil} and DT ($bmep$=5 bar, n=2000 rpm).

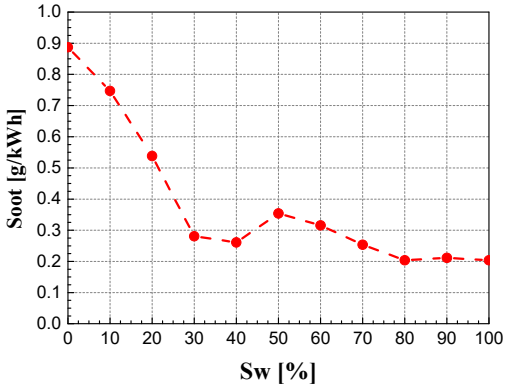

Figure 12. Soot versus Sw at DT=1200 µs and ET_{pil}=190 µs ($bmep$=5 bar, n=2000 rpm).

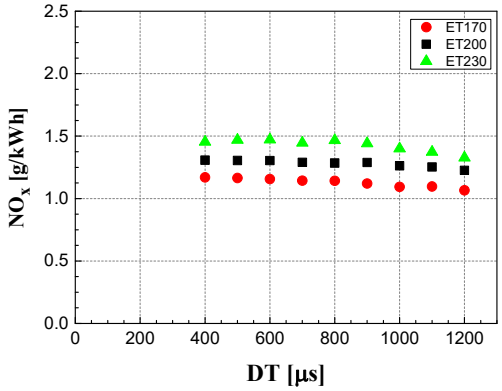

Figure 13. NO_x versus DT for different ET_{pil} values ($bmep$=8 bar, n=2500 rpm)

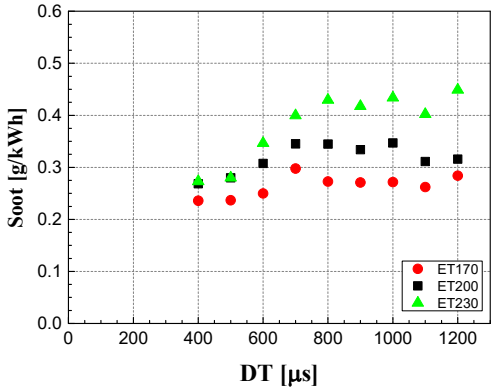

Figure 14. Soot versus DT for different ET_{pil} values ($bmep$=8 bar, n=2500 rpm).

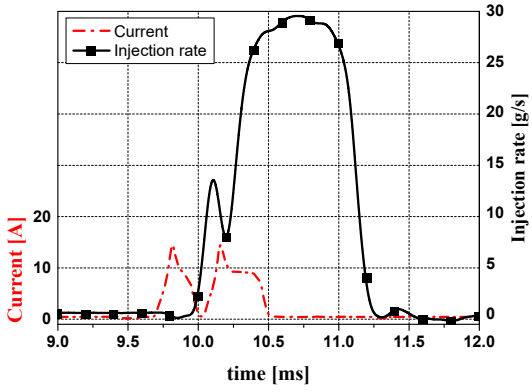

Figure 15. Rate-shaped main injection by means of pre and main fusion (p_{rail} = 1000 bar, ET_{Pre} = 250 µs, DT_{Pre}= 110 µs, ET_{Main} = 400 µs).

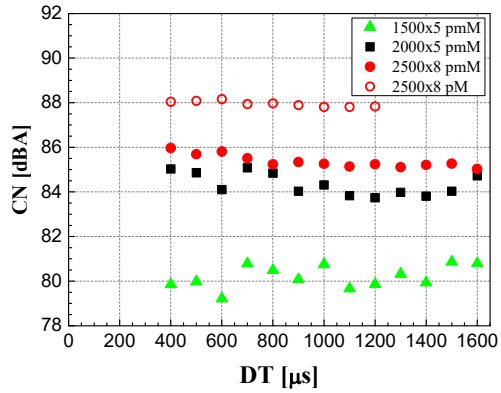

Figure 16. CN versus DT_{Pil} at different engine points for the pmM and pM strategies.

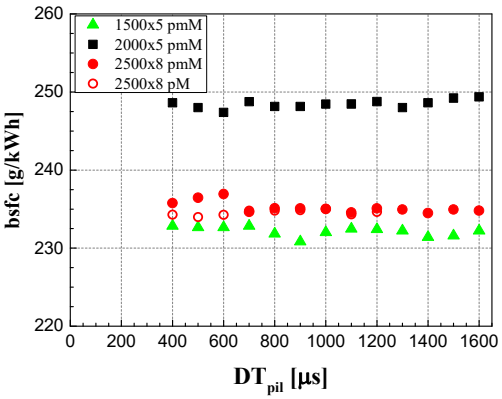

Figure 17. *bsfc* versus DT_{Pil} at different engine points for the *pmM* and *pM* strategies

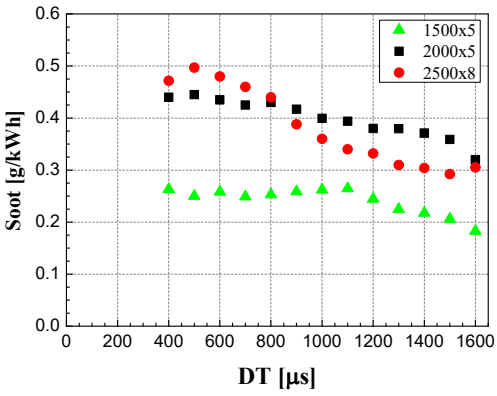

Figure 18. Soot versus DT_{Pil} at different engine points for the *pmM* strategy.

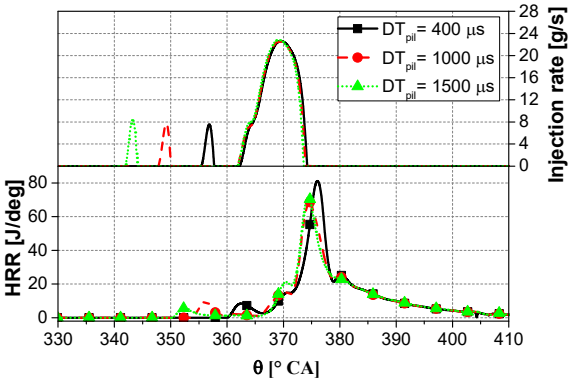

Figure 19. *HRR* and injected flow-rate versus θ traces for distinct DT_{Pil} values for the *pmM* strategy (*bmep*=5 bar, *n*=2000 rpm).

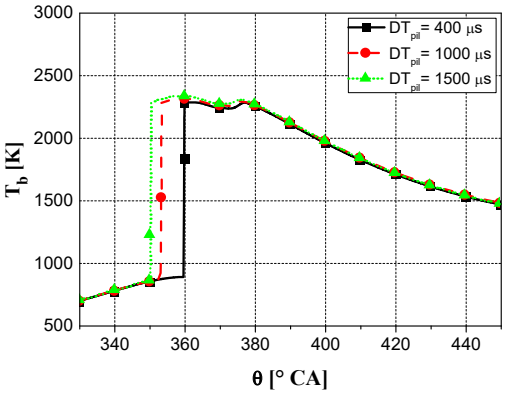

Figure 20. T_b versus θ distributions for distinct DT_{Pil} values for the *pmM* strategy (*bmep*=5 bar, *n*=2000 rpm).

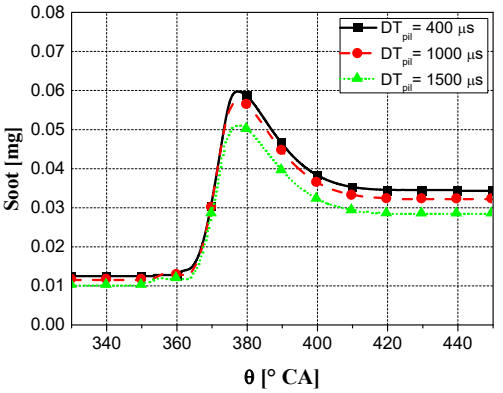

Figure 21. Soot versus θ distributions for distinct DT_{Pil} values values for the pmM strategy (bmep=5 bar, n=2000 rpm).

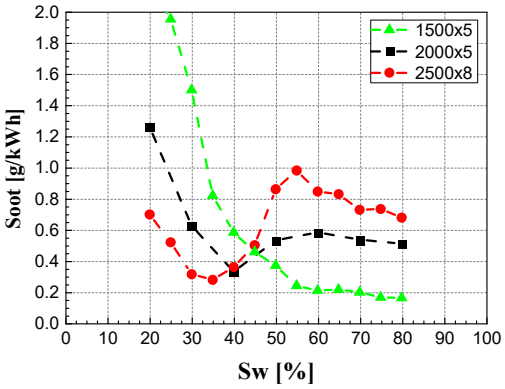

Figure 22. Soot versus *Sw* for different engine points for the *pmM* strategy.

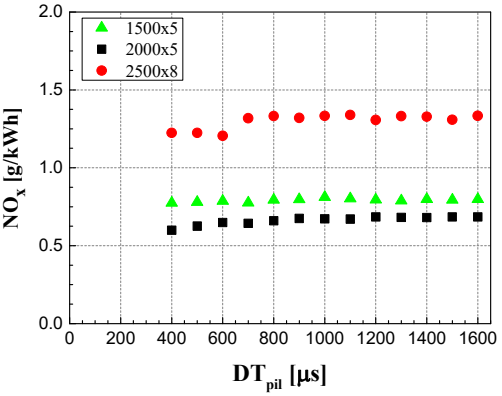

Figure 23. NO_x versus DT_{Pil} for different engine points for the *pmM* strategy.

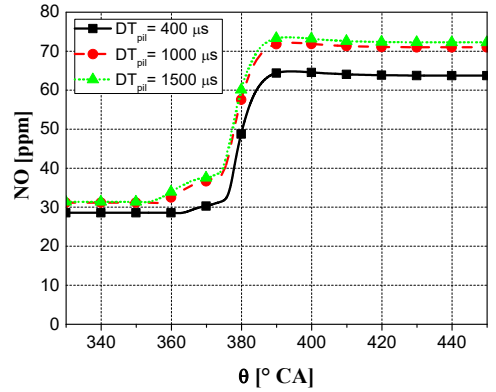

Figure 24. *NO* versus θ distributions for distinct DT_{Pil} values for the *pmM* strategy (*bmep*=5 bar, *n*=2000 rpm

617